JOURNAL OF MATERIALS SCIENCE 33 (1998) 2269–2281

Effect of inclusions on the tensile properties of Al–7% Si–0.35% Mg (A356.2) aluminium casting alloy

L. LIU, F.H. SAMUEL
Département des Sciences appliquées, Université du Québec à Chicoutimi, 555, boul. de l'Université, Chicoutimi(Québec), Canada G7H 4A4

The present study was performed on an A356.2 alloy. Two types of initial materials were used, i.e. fresh and recycled. A total of 13 operations representing those normally applied in aluminium foundries were simulated under dry atmospheric conditions (humidity ~15%–20%). The molten metal was cast into test bars which were T6 tempered prior to tensile testing. The results show that holding the liquid metal for a long time, i.e. 72 h at 735 °C leads to sedimentation of most inclusions towards the bottom of the melting crucible. However, a change in the surrounding humidity may cause absorption of hydrogen and, hence, a large amount of porosity. Degassing using dry argon injected into the liquid metal through a rotary impeller (speed ~160 r.p.m) appears to be the best technique for inclusion removal. The efficiency of this process is significantly improved when it is coupled with filtration using ceramic foam filters (10 and 20 p.p.i). A linear relationship between alloy ductility and logarithm of percentage inclusions has been established. Owing to decohesion between the inclusions/oxide films and the surrounding matrix, cracks are easily initiated at their interfaces, leading to unpredicted failure. © *1998 Chapman & Hall*

1. Introduction

The detrimental effects of the presence of inclusions in aluminium are well documented [1–8]. Although much work has been reported on the study of inclusions, the problem of measuring metal cleanliness through a sensitive quantitative method still exists. The difficulty is further compounded by the fact that the inclusions to be measured are usually very small, about 10–20 μm in diameter, and present in trace amounts (about 10 p.p.m). The main inclusions that occur during the melting of aluminium alloys or holding periods prior to casting are aluminium oxide (Al_2O_3) as dispersed particles or oxide films, aluminium carbide (Al_4C_3), magnesium oxide (MgO), spinel ($MgAl_2O_4$), titanium diboride (TiB_2), aluminium boride (AlB), and titanium aluminide ($TiAl_3$) [1–8].

Many studies have been conducted on the role of non-metallic inclusions and oxide films in determining the alloy mechanical properties. The presence of oxide films can lead to a significant scatter in the tensile properties of the cast alloy due to early initiation of fracture. Removal of such inclusions/oxides is expected to result in more consistent and reproducible mechanical properties.

Samuel *et al.* [9] studied the effect of melt cleanliness on the mechanical properties of a 359 aluminium alloy reinforced with 20% SiC particles (average particle size ~20 μm). Their work shows that the percentage elongation varies linearly with the volume fraction of inclusions/oxides, and can be expressed by the relationship

$$\% \text{ elongation} = 1.06 - 0.66X \quad (1)$$

where X represents the volume fraction of inclusions.

Campbell [10] has reported that the oxide films that remain in the cast product will cause mechanical weakness and form leak paths that emerge through the walls of the casting. In some cases, the large amount of porosity associated with the oxide films can further enhance the weakness. Fractographic observations reveal that crack initiation is related to the presence of these inclusions. Spinel inclusions are often seen to be surrounded by partial or complete voids, indicating debonding between the inclusions and the matrix during fracture.

Hedjazi *et al.* [11] examined the effect of non-metallic inclusions on the tensile properties of an Al–4.5% Cu–1.5% Mg alloy. Their study showed that inclusions which arise as a result of various physical and chemical phenomena that occur during the melting and casting process were found to be non-uniformly distributed within the cast product. Categorizing the inclusions/oxides as two types, namely, film and non-film, and further classifying the latter type according to their size as macro-inclusions (> 50 μm) and micro-inclusions (< 50 μm), the authors concluded that both film and non-film inclusions lower the ductility, i.e. percentage elongation, to a greater extent

than the strength of the alloy. In their opinion, filtration improves with bed depth as do the tensile properties [12].

Arai *et al.* [13] have observed that molten metal filtration increases the strengths of 2014, 2017 and 7075 extrusions. The reason is a decrease in the non-metallic inclusions which disturb homogeneous precipitation. Ductilities of extrusions also increase by molten metal filtration. The non-metallic inclusions act as nucleation sites for dimple cleavages [13]. Rios *et al.* [14] attribute the lower ductility and strength in the transverse direction (deformation axis normal to extrusion axis and tube radius) in hot-extruded AA2014 aluminium tube specimens to the influence of coarse inclusions that fracture early during tensile deformation. The resultant cracks induce void formation around the small inclusions in the matrix.

The role of inclusions in initiating fatigue cracks under dynamic loading is well documented. Chien *et al.* [15] report that $TiAl_3$ particles nucleate cracks in A201 alloys. It is expected that other types of inclusions may act in the same way, particularly if their size is large. Gerold [16] also found that in commercial alloys, intermetallic inclusions are additional sources for crack initiation. Thus, filtered metal should produce castings having an increased fatigue resistance.

The present paper documents the tensile test results obtained from a study of Al–7% Si–0.35% Mg (A356.2) alloy, where a total of 13 operations, typical of those customarily used in the aluminium industry, were applied to the alloy melts, to investigate the type and amount of inclusions that could occur as a result of these operations, and their influence on the tensile properties, in particular, the alloy ductility.

2. Experimental procedure

The A356.2 alloy used in the present study was supplied by Guelph Foundry Works, Alcan International Limited in the form of 12.5 kg ingots. The chemical composition of the as-received alloy is shown in Table I. The ingots were cut, cleaned, and melted in a silicon carbide crucible of 28 kg capacity, using an electrical resistance furnace. The melting temperature was held at $735 \pm 5\,^{\circ}C$. The maximum humidity was about 15%. No degassing was applied. The hydrogen level was $\leqslant 0.1\,ml/100\,g$ Al as measured by an Alscan™ apparatus. Prior to casting, melt-treatment agents such as strontium (400 p.p.m. Sr, added as Al–10% Sr master alloy) or TiB_2 (in the form of Al–5% Ti–1% B, measured in terms of a 0.02 wt % Ti addition) were added to the melt.

Casting was done in a Stahl permanent mould (type ASTM B-108) heated at 425 °C. The test bars obtained from the Stahl mould castings were solution heat treated for 8 h at 540 °C, in a forced-air furnace, followed by quenching in hot water (60 °C). The quenched test bars were stabilized at room temperature for 24 h prior to hardening at 150 °C for 5 h.

The solution treated test bars were pulled to fracture at room temperature in an Instron Universal testing machine at a strain rate of $4 \times 10^{-4}\,s^{-1}$. A strain gauge extensometer (50 mm range) was attached to the test specimen for measuring the alloy ductility. The data were analysed using a special software designed for this work. Tensile properties, namely yield stress (YS) at 0.2% offset strain, ultimate tensile strength (UTS), and fracture elongation (EL%) were derived from the data aquisition system. The volume fraction of non-metallic inclusions was measured from macrophotographs of the specimen fracture surfaces, using the grid method.

TABLE I Chemical composition (wt %) of A356.2 alloy

Si	Mg	Fe	Mn	Cu	Be	Sr
6.78	0.33	0.11	0.04	0.02	–	–

3. Results and discussion

3.1. Fresh alloy

The experimental conditions applied in the present work are summarized in Table II, while tensile test data are listed in Tables III–X.

It can be seen from Table III that a settling time of 72 h enhances the alloy properties, in particular, percentage elongation, which reaches almost 18%. It is important to note the uniformity of the tensile properties of all castings regardless of the casting sequence. Vigorous stirring appears to push the inclusions that settle close to the bottom of the crucible towards the upper surface of the molten metal. Depending upon the stirring speed and time, the thickness of the contaminated portion near the melt surface increases as shown in Table IV, where the first six castings exhibit low ductility.

Degassing, on the other hand, is very effective in removing most of the inclusions and results in a marked improvement in the tensile properties (12%–20% EL) for most of the castings, Table V. However, if the inclusions in the upper portion of the liquid metal following the degassing are not skimmed immediately, these inclusions (with heavier densities compared to that of liquid aluminium) tend to settle down towards the bottom of the crucible. Depending upon the settling time, the molten metal will become contaminated again, leading to unpredictable results. Table VI shows that in some cases, when the settling time after degassing is large, e.g. 4 h, two test bars produced simultaneously from the same casting can possess completely different ductilities, the latter being controlled by the motion of inclusions during filling of the mould, as shown schematically in Fig. 1.

Filtration using ceramic foam filters is one of the most effective methods for inclusion removal. This technique is now being applied in most aluminium foundries [17–22]. In the present work, round filter discs (50 mm diameter, 15 mm thickness) were mounted at the bottom of cylindrical stainless steel tubes. Both the tube(s) and filter(s) were preheated at 450 °C, and placed firmly at the top of the sprue of the Stahl mould prior to casting. The molten metal was poured through such tubes. Table VII shows the consistency

TABLE II Melt conditions for preparation of tensile test bars

Experiment	Type of charge	Weight of charge (kg)	Melt temperature (°C)	Mould temperature (°C)	Additive	Settling time (h)	Stirring speed (r.p.m.)	Stirring time (min)	Degassing time (min)	Filter size (p.p.i)	Humidity (%)
3	Fresh	18	735 ± 5	435 ± 3	–	72	–	–	–	–	18
4	Fresh	18	735 ± 5	435 ± 3	–	0	125–130	20	–	–	15
5	Fresh	18	735 ± 5	435 ± 3	–	0	125–130	–	45	–	17
15	Fresh	18	735 ± 5	435 ± 3	–	4[a]	125–130	–	45	–	13
6A–6G	Fresh	25	735 ± 5	435 ± 3	–	0	–	–	–	10	17
6H–6N	Fresh	25	735 ± 5	435 ± 3	–	0	125–130	–	45	10	17
9A–9F	Fresh	20	735 ± 5	435 ± 3	Al–Ti–B	1[a]	125–130	15	–	–	17
9G–9L	Fresh	20	735 ± 5	435 ± 3	Al–Ti–B	0	125–130	–	45	–	17
7A–7H	Fresh	25	735 ± 5	435 ± 3	Al–Sr	0	125–130	15	–	–	21
7I–7P	Fresh	25	735 ± 5	435 ± 3	Al–Sr	0	125–130	–	45	–	21
8A–8E	Fresh	25	735 ± 5	435 ± 3	–	72[a]	125–130	15	–	–	16
8F–8J	Fresh	25	735 ± 5	435 ± 3	–	0	–	–	–	10	16
8K–8O	Fresh	25	735 ± 5	435 ± 3	–	0	125–130	–	45	–	20
11	Scrap	20	735 ± 5	435 ± 3	–	0	–	–	–	–	19
10	Scrap	20	735 ± 5	435 ± 3	–	72	–	–	–	–	15
12A–12F	Scrap	20	735 ± 5	435 ± 3	–	0	125–130	20	–	–	15
12G–12L	Scrap	20	735 ± 5	435 ± 3	–	0	125–130	–	45	–	15
14A–14F	Scrap	20	735 ± 5	435 ± 3	–	72[a]	125–130	15	–	–	17
14G–14K	Scrap	20	735 ± 5	435 ± 3	–	0	125–130	–	45	–	17
13A–13G	Scrap	20	735 ± 5	435 ± 3	–	0	–	–	–	10	20
13H–13N	Scrap	20	735 ± 5	435 ± 3	–	0	125–130	–	45	10	20

[a] Stirring/degassing before settling.

in tensile properties for castings marked 6A to 6G, which were obtained following such a procedure. The combined effect of degassing and filtering resulted in ductilities as high as 16%, especially for the last castings in the casting sequence, i.e. those taken from the melt towards the bottom of the melting crucible.

Grain refining of an Al–Si casting is normally done through the addition of small amounts of TiB_2 to the melt in the form of Al–Ti–B master alloys [23–26]. Various types of master alloys can be used, such as Al–10% Ti–1% B, Al–5% Ti–1% B, and Al–7.5% Ti–7.5% B. In the present work, Al–5% Ti–1% B was chosen, being commonly used in aluminium foundries. The amount needed to be added was calculated on the basis of a 0.02 wt % Ti addition. As was observed earlier in our study, such a small amount of Al–Ti–B master alloy is enough to introduce an extremely large number of TiB_2 particles into the melt. These particles act as nucleants for the crystallization of the liquid metal during solidification. Table VIII depicts the maximum tensile properties (castings A–C) and minimum tensile properties (castings D–F), with respect to percentage elongation. It can be seen that although the alloy strength is high, the associated ductilities do not necessarily follow the same trend. Degassing the second half of the liquid metal (i.e. that in the lower portion of the crucible) did not necessarily reduce the difference in percentage elongation obtained from the two test bars produced simultaneously from the same casting. This observation has been explained schematically in Fig. 2, where the amount of clean metal (or rather, its depth with respect to the crucible diameter) after degassing is much less than what would be expected from the thickness of the dross and inclusion-rich layers.

Modification of A356.2 alloy with strontium in the range of 250–300 p.p.m. is recommended in order to change the eutectic silicon morphology from acicular to fibrous and enhance the alloy properties [27–31]. This type of melt treatment is expected to shorten the solution heat-treatment time required to achieve more or less complete spheroidization of the eutectic silicon particles. However, the addition of strontium causes a significant increase in the porosity volume fraction which, in turn, affects the alloy strength. Table IX depicts the tensile properties of strontium-modified alloy obtained in the present study. Apparently, degassing leads to contamination of the liquid metal due to the reason mentioned above.

When the liquid metal is held at a sufficiently high temperature, e.g. 735 °C, for a lengthy period of time ($\sim$72 h), most of the inclusions will settle to the bottom of the crucible. Thus, it is expected that the upper portion of the liquid metal (i.e. that in the upper one-third of the crucible) is reasonably clean, Table X. Using ceramic foam filters for the next one-third portion of the melt proved to be effective in removing the settled inclusions. As the amount of liquid metal remaining thereafter was fairly little, degassing resulted in disturbing the settled inclusions at the bottom of the crucible, and, hence, random ductilities.

3.2. Recycled (scrap) alloy

The recycled material used in the present work consisted of a mixture of gates and runners collected from the fresh alloy castings (except those containing TiB_2 and strontium), as well as any remaining metal that was not used for making test bars. The main type of inclusions observed in the recycled (scrap) alloy was

TABLE III Tensile test results of experiment 3 (fresh alloy)

Experiment	YS (MPa)	UTS (MPa)	% Elongation
3A1	108.472	271.125	12.62
3A2	106.018	264.933	11.681
3B1	101.294	253.005	12.61
3B2	101.612	253.729	9.25
3C1	98.833	247.075	11.47
3C2	106.286	263.865	13.52
3D1	103.818	259.404	9.15
3D2	106.066	264.851	9.95
3E1	103.777	259.424	14.61
3E2	103.273	257.315	13.81
3F1	106.852	265.382	15.81
3F2	103.073	257.611	10.91
3H1	107.590	268.815	16.81
3H2	109.024	272.518	12.51
3I1	109.555	273.690	15.51
3I2	107.507	268.484	11.483
3J1	121.635	277.827	19.15
3J2	106.528	265.271	11.18
3K1	112.195	277.620	17.91
3K2	107.479	268.560	14.12

TABLE IV Tensile test results of experiment 4 (fresh alloy)

Experiment	YS (MPa)	UTS (MPa)	% Elongation
4A1	102.156	254.929	5.67
4A2	109.093	272.725	7.95
4B1	113.395	281.785	7.409
4B2	112.347	280.599	6.758
4C1	111.692	279.179	7.375
4C2	102.005	254.688	4.933
4D1	116.808	291.852	11.12
4D2	114.009	284.777	8.197
4E1	110.872	277.172	10.05
4E2	111.334	278.124	8.267
4F1	108.672	271.732	14.36
4F2	112.326	280.606	10.81
4G1	112.389	280.957	14.63
4G2	109.320	273.242	12.65
4H1	112.451	281.006	12.45
4H2	115.933	289.418	13.77
4I1	108.376	270.801	14.81
4I2	117.773	294.065	13.71
4J1	117.056	291.783	13.56
4J2	114.609	282.074	10.51
4K1	107.135	267.781	15.11
4K2	115.919	289.507	12.65
4L2	117.146	292.472	16.91

TABLE V Tensile test results of experiment 5 (fresh alloy)

Experiment	YS (MPa)	UTS (MPa)	% Elongation
5A1	125.420	299.926	12
5A2	115.091	287.570	16.97
5B1	117.277	293.065	6.321
5B2	118.649	296.347	10.786
5C1	111.375	278.310	12.17
5D1	115.691	287.556	13.97
5D2	111.678	278.923	8.163
5E1	129.985	295.230	11.08
5E2	104.963	262.148	9.25
5F1	101.198	252.791	13.06
5F2	116.601	291.155	16.71
5G1	116.450	291.100	10.604
5G2	117.580	293.189	14.17
5H1	119.097	297.492	12.85
5H2	118.994	296.554	13
5I1	120.545	297.154	12.06
5J1	119.401	297.540	15.52
5J2	115.684	288.611	16.88
5K1	115.877	289.487	19.05
5K2	121.359	300.188	16.5

TABLE VI Tensile test results of experiment 15 (fresh alloy)

Experiment	YS (MPa)	UTS (MPa)	% Elongation
15A1	113.961	284.522	9.691
15A2	112.588	281.192	10
15B1	115.071	287.384	16
15B2	115.071	287.625	10.2
15C1	114.554	286.370	14.1
15C2	114.236	284.867	10.41
15D1	113.795	284.302	16.5
15D2	103.246	257.618	5.423
15E1	114.429	285.501	14.2
15E2	115.933	289.652	10.25
15F1	112.726	281.219	16.9
15G1	115.912	289.507	15
15G2	103.990	259.390	4.238
15H1	107.900	268.091	13.2
15H2	106.411	265.706	5.29
15I1	116.167	289.983	14.7
15I2	104.549	261.031	7.75
15J1	103.349	257.852	16.7
15J2	110.389	275.635	13.5
15K1	111.168	277.407	11.7
15K2	114.905	287.087	12.8
15L1	115.774	288.928	12.4
15L2	113.561	283.867	10

the large number of oxide films that floated to the surface during melting. Tables XI–XV summarize the tensile properties that were obtained following several foundry operations.

Table XI exemplifies the effect of oxide films on the alloy strength immediately after melting. As can be seen, the ductility improved gradually along the length of the melting crucible. Holding the liquid metal at 735 °C for a period as long as 72 h led to flotation of most of the oxide films to the upper surface of the molten metal which could be removed easily, and sedimentation of heavy inclusions to the bottom of the crucible. This process resulted in elongations that ranged between 12% and 18%, Table XII, compared to 5%–14% shown in the previous case, Table XI.

One of the serious problems that could occur during melting is if the melt is vigorously stirred: such an operation would disturb a large portion of the oxide films in suspension near the upper surface of the liquid metal, and incorporate them into the bulk of the melt. Their concentration within the melt will determine the alloy properties, Table XIII. These properties are found to be more or less comparable with those shown in Table XI. Thus, degassing may be the better way to remove both inclusions and oxide films. The

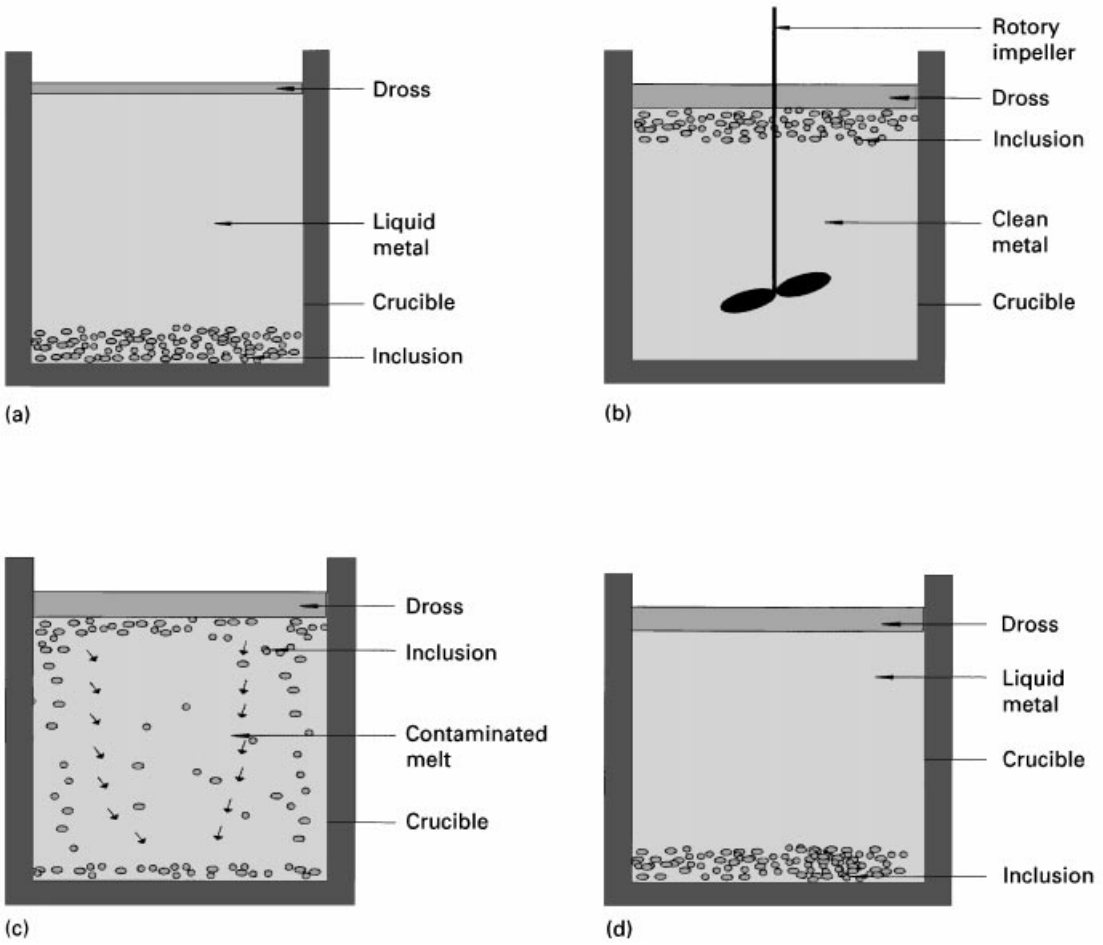

Figure 1 Schematic diagram showing the motion of inclusions before and after degassing. (a) After melting (experiment 6.11), (b) after degassing (experiment 5), (c) after degassing + settling 4 h (experiment 15), (d) after degassing/stirring + settling 72 h (experiment 3.1).

TABLE VII Tensile test results of experiment 6 (fresh alloy)

Experiment	YS (MPa)	UTS (MPa)	% Elongation
6A1	110.975	277.303	11.1
6A2	117.463	293.451	11.05
6B1	117.029	288.776	8.63
6B2	119.325	291.700	12.13
6C1	112.078	279.847	12.77
6D2	125.730	282.985	9.27
6E1	116.994	292.045	7.95
6E2	111.961	278.613	10.07
6F1	111.313	277.448	7.503
6F2	119.415	298.347	13.86
6G1	116.477	290.217	8.92
6G2	114.705	285.356	11.13
6H1	108.927	271.580	6.9
6H2	118.173	289.128	13.78
6I1	121.945	288.818	12.74
6I2	114.209	284.791	14.55
6J1	117.822	293.155	11.46
6J2	115.533	287.522	11.112
6K1	120.890	301.725	12.68
6K2	115.319	287.632	9.85
6L1	116.257	288.894	17.18
6L2	123.345	304.483	14.68
6M1	116.201	286.632	9.36
6M2	115.602	288.852	7.834
6N1	116.498	289.576	14.92
6N2	113.899	284.060	17.15

TABLE VIII Tensile test results of experiment 9 (fresh alloy)

Experiment	YS (MPa)	UTS (MPa)	% Elongation
9A1	117.312	292.948	9.9
9A2	114.278	285.522	7.843
9B1	108.314	270.553	6.116
9B2	114.519	286.122	6.664
9C2	116.077	290.100	9.2
9D1	116.070	289.893	7.987
9D2	112.071	279.296	8.136
9E1	115.436	288.432	9.27
9E2	116.836	291.941	12.3
9F2	118.249	294.010	11.5
9G1	116.001	289.700	9.6
9G2	113.492	283.460	9.3
9H1	112.906	281.144	6.967
9H2	107.403	268.498	5.466
9I1	119.256	295.809	11.5
9I2	111.258	278.082	7.23
9J1	116.181	290.273	9.35
9J2	154.924	386.803	11.25
9K1	113.402	283.185	14
9K2	116.367	290.852	15.8
9L1	117.236	292.996	9.9
9L2	116.112	289.838	13.6

effectiveness of the degassing process will depend directly on the amount of molten metal.

The combined effect of sedimentation (72 h at 735 °C) and degassing on the alloy tensile properties is

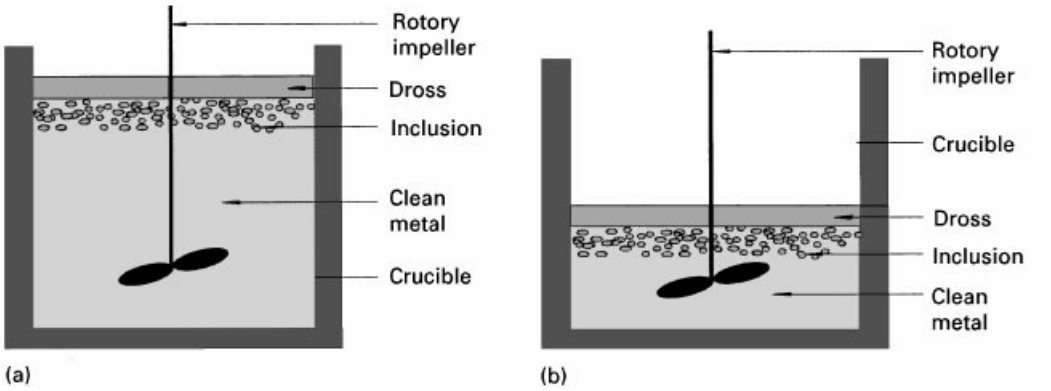

Figure 2 Schematic diagram showing the effectiveness of degassing with respect to amount of liquid metal. (a) Full crucible (experiment 5), (b) partially full crucible (experiments 6, 7, 9).

TABLE IX Tensile test results of experiment 7 (fresh alloy)

Experiment	YS (MPa)	UTS (MPa)	% Elongation
7A1	113.133	282.654	9.2
7A2	112.726	281.475	10.65
7B1	116.643	291.017	11.7
7B2	111.478	278.655	11.532
7C1	106.673	266.347	7.519
7C2	115.450	288.294	9.4
7D1	107.155	267.685	7.755
7D2	112.754	281.702	11.25
7E1	110.237	275.504	7.216
7E2	113.974	284.708	10.5
7F1	113.692	284.040	8.982
7F2	115.153	287.570	13.45
7G1	106.479	266.064	6.49
7G2	113.678	283.791	8.759
7H1	110.823	276.490	8.499
7H2	116.581	290.969	13.4
7I1	109.368	273.063	13.35
7J1	106.652	266.526	7.414
7J2	113.202	282.854	10.4
7K1	98.199	245.221	5.485
7K2	110.148	274.883	9.15
7L1	99.460	248.620	5.923
7L2	104.673	261.617	7.8
7M1	99.033	247.482	3.705
7M2	114.960	287.342	12.5
7N2	117.580	293.465	12
7O1	96.847	242.097	4.441
7O2	111.085	277.386	10.65
7P1	99.488	248.365	4.232
7P2	104.039	259.707	11.3

TABLE X Tensile test results of experiment 8 (fresh alloy)

Experiment	YS (MPa)	UTS (MPa)	% Elongation
8A1	112.892	282.061	7.95
8A2	107.445	268.471	6.441
8B1	115.650	288.880	14.5
8B2	114.416	285.991	9.75
8C1	103.404	258.238	4.18
8C2	110.492	275.807	9.176
8D1	112.154	280.309	9.7
8D2	111.409	278.344	6.151
8E1	111.485	278.537	9.3
8E2	110.734	276.800	10.9
8F2	113.836	284.122	8.319
8G1	110.630	276.372	10.5
8G2	113.299	282.895	9.023
8H1	114.443	283.626	12
8H2	109.300	273.056	6.9
8I1	115.084	287.618	8.413
8I2	110.113	275.145	6.749
8J1	115.960	289.280	10.8
8J2	111.451	278.441	6.982
8K1	96.254	240.146	2.659
8K2	113.685	283.984	10.95
8L1	91.641	228.080	2.214
8L2	111.382	278.386	6.98
8M1	89.366	223.405	1.937
8M2	112.223	280.392	7.459
8N1	108.913	272.228	7.431
8N2	112.582	281.433	10.7
8O1	95.744	238.767	2.371
8O2	113.519	283.467	6.546

shown in Table XIV. It is interesting to note the role of settling time in improving the tensile properties of the castings corresponding to the upper portion of the crucible, whereas degassing tends to enhance the ductilities of castings made from metal close to the crucible bottom. Casting 14G is a good example of inclusion concentration caused by inclusion floatation.

Filtration of liquid aluminium with 10 p.p.i. ceramic foam filters is an important process of inclusion/oxide removal. Table XV shows that, due to floatation of oxide films to the upper surface of the liquid metal, filtration with 10 p.p.i. filters might not be very effective, and a finer filter size (i.e. 20 p.p.i.) would be more appropriate. It is also observed that the alloy elongation improves gradually with increasing casting sequence. Applying degassing reduces the tensile properties of the first casting (i.e. 13H), as explained schematically in Fig. 8 (see later). Beyond that, the alloy exhibits consistent improvement (13L).

Table XVI and XVII summarize the average tensile properties of the A356.2 alloy studied for the different experimental conditions listed in Table II.

For castings made from fresh ingots, degassing of a large quantity of liquid metal (namely, a full crucible in the present case) seems to be the best method for inclusion removal and, hence, for achieving the highest percentage elongation. However, when applied to

TABLE XI Tensile test results of experiment 11 (scrap alloy)

Experiment	YS (MPa)	UTS (MPa)	% Elongation
11A1	98.102	245.152	4.585
11A2	103.377	258.176	5.088
11B1	105.562	263.610	7.116
11B2	100.219	250.447	4.663
11C1	106.452	169.955	7.372
11C2	103.680	258.866	5.424
11D1	109.844	273.159	6.908
11D2	110.934	277.069	9.12
11E1	113.650	283.764	10.4
11E2	113.747	284.357	10
11F1	111.223	277.600	12.05
11F2	111.961	279.634	10.223
11G1	110.541	276.303	8.845
11G2	104.901	261.948	5.58
11H1	111.651	278.827	8.34
11H2	96.930	242.256	10.2
11I1	113.981	176.409	11.02
11I2	110.423	275.759	10.3
11J1	110.954	277.055	13.4
11J2	113.623	284.019	14.45
11K1	111.010	277.158	14.2
11K2	112.320	280.316	13.1
11L1	109.341	273.152	10.5
11L2	113.974	284.481	10.8

TABLE XII Tensile test results of experiment 10 (scrap alloy)

Experiment	YS (MPa)	UTS (MPa)	% Elongation
10A1	110.803	276.517	16.5
10A2	113.119	282.688	10
10B1	112.844	281.730	14.5
10B2	107.672	269.084	7.285
10C1	114.540	286.280	9.449
10C2	114.871	287.073	11.9
10D1	113.657	283.481	13.4
10D2	115.622	288.632	14.8
10E1	114.085	284.681	14.5
10E2	113.864	284.570	15.9
10F1	111.465	278.165	10.5
10F2	113.726	282.006	12.4
10G1	111.340	278.227	9.4
10G2	109.224	272.118	6.285
10H1	114.629	285.536	13.6
10H2	112.264	280.392	11.2
10I1	109.996	274.400	13
10I2	115.140	287.459	10.8
10J1	112.540	281.102	10.6
10J2	111.878	279.606	8.232
10K1	97.054	242.449	16
10K2	111.230	277.586	11.6
10L1	113.064	282.399	15.8
10L2	112.526	281.233	15.8
10M1	107.714	269.070	12.9
10M2	112.609	281.330	14.8

a very limited amount of liquid metal, degassing causes liquid contamination, instead, leading to the lowest values of elongation observed. When the castings are made from recycled materials, the obtained ductilities are more or less the same, regardless of the type of melt treatment. This observation may be explicable in terms of the large amounts of oxide films present in the recycled alloy melts.

TABLE XIII Tensile test results of experiment 12 (scrap alloy)

Experiment	YS (MPa)	UTS (MPa)	% Elongation
12A1	110.417	275.800	7.57
12A2	110.334	275.676	6.405
12B1	108.582	271.229	7.155
12B2	106.769	266.892	7.506
12C1	106.390	265.782	10.8
12C2	111.616	278.999	8.039
12D1	112.216	280.323	9.4
12D2	111.630	278.965	9.042
12E1	113.912	284.481	11.6
12E2	114.243	181.821	10.25
12F1	114.188	285.122	13.1
12F2	112.782	281.668	12.1
12G1	115.043	287.473	12.3
12H1	114.540	286.170	11.6
12H2	112.382	280.840	8.9
12I1	114.416	285.894	9.8
12I2	120.497	298.443	12.7
12J1	116.015	289.480	17.5
12J2	115.484	288.632	15.5
12K1	111.982	279.785	11.1
12K2	114.809	286.949	12.35
12L1	110.610	276.276	11.4
12L2	113.381	277.255	14.2

3.3. Ductility–percentage inclusions/oxide films relationship

Fig. 3a–g show the size and distribution of non-metallic inclusions/oxide films found on the fracture surfaces of test bars obtained from fresh ingots. The corresponding elongations range from 19%–1.5%. Similarly, Fig. 4 shows the oxides observed on the fracture surfaces of test bars obtained from scrap. The area fraction of inclusions/oxides was measured from photographs similar to those shown in Figs 3 and 4, using the grid method. The relationship between percentage elongation and log area percentage inclusions/oxide films is presented in Fig. 5. A linear relationship expressed as

$$\text{percentage elongation} = 9.5 - 2.98 \log \text{area percentage inclusions/oxide films} \quad (1)$$

is obtained, with a good fitness coefficient ($R^2 \sim 0.9$) .

Table XVIII lists the total inclusions, harmful inclusions and oxide films as measured by the PoDFA technique [32, 33], and the corresponding tensile properties measured for similar melt experimental conditions. It is evident from this table that the oxide films have a far more deleterious effect on the mechanical properties. This observation is in accordance with the oxides shown in Figs 3 and 4.

3.4. Fractography

As shown in our previous work [32, 33], the main oxide inclusions in A356.2 alloy melts held for a long period, i.e. 72 h, at 735 °C are aluminium oxide (Al_2O_3) and spinel ($MgAl_2O_4$). Owing to plastic deformation during tensile loading, these oxides tend to break into small fragments that are segregated in

TABLE XIV Tensile test results of experiment 14 (scrap alloy)

Experiment	YS (MPa)	UTS (MPa)	% Elongation
14A1	95.338	256.853	10.9
14A2	95.472	257.280	11.3
14B1	89.204	240.008	5.761
14B2	92.296	248.951	7.869
14C1	93.389	251.702	11.9
14C2	93.146	250.585	12.5
14D1	95.977	258.487	13.3
14D2	93.466	252.061	9.598
14E1	95.779	258.259	12.2
14E2	93.811	252.915	8.803
14F1	97.536	262.893	11.3
14F2	95.127	256.418	10.4
14G1	91.268	245.965	5.208
14G2	93.696	252.233	10.4
14H1	95.133	256.584	11.9
14H2	92.859	250.392	9.2
14I1	93.964	253.302	12.7
14I2	84.265	227.204	5.975
14J1	93.593	252.288	8.374
14J2	95.344	256.984	13.2
14K1	92.462	249.365	15.4
14K2	91.549	246.710	13.6

TABLE XV Tensile test results of experiment 13 (scrap alloy)

Experiment	YS (MPa)	UTS (MPa)	% Elongation
13A1	107.583	268.905	5.382
13A2	107.955	269.663	5.604
13B1	107.203	267.988	9
13B2	70.805	176.919	8.741
13C1	115.153	287.859	10.9
13C2	110.251	275.441	5.938
13D1	118.373	295.775	9.3
13D2	115.422	288.259	10.3
13E1	117.684	293.927	10.9
13E2	109.079	272.449	11.35
13F1	115.298	287.590	11.3
13F2	113.050	282.619	9.95
13G1	117.305	293.189	14.3
13G2	114.043	285.060	10.9
13H1	111.340	278.034	9.2
13H2	102.763	256.797	7.996
13I1	116.684	291.493	7.934
13I2	115.229	287.997	13.7
13J1	103.515	258.356	12.3
13K2	115.071	287.473	9.6
13L1	115.181	287.770	9.5
13L2	116.153	290.080	13.25

TABLE XVI Average tensile properties (fresh alloy)

Experiment	YS (MPa)	UTS (MPa)	% Elongation
3	106.54 ± 4.8	264.53 ± 8.27	13.20 ± 2.79
4	111.86 ± 4.34	279.186 ± 10.69	11.03 ± 3.4
5	116.65 ± 6.28	288.72 ± 12.35	17.59 ± 19.65
15	111.18 ± 5.11	277.56 ± 12.83	11.42 ± 4.02
6A–6G	116.12 ± 4.29	286.34 ± 7.08	10.37 ± 1.98
6H–6N	116.76 ± 3.64	289.06 ± 7.72	12.44 ± 3.2
9A–9F	114.92 ± 2.9	286.88 ± 7.16	8.89 ± 1.97
9G–9L	117.88 ± 12.08	294.22 ± 30.11	10.33 ± 3.07
7A–7H	112.29 ± 3.29	280.44 ± 8.15	9.77 ± 2.12
7I–7P	106.05 ± 6.82	264.90 ± 16.99	8.45 ± 3.32
8F–8J	112.68 ± 2.37	281.17 ± 5.68	8.85 ± 1.89
8K–8O	104.53 ± 9.98	261.03 ± 25.12	5.92 ± 3.45

TABLE XVII Average tensile properties (scrap alloy)

Experiment	YS (MPa)	UTS (MPa)	% Elongation
11	108.68 ± 5.1	262.89 ± 30.27	9.32 ± 2.99
10	111.83 ± 3.67	279.15 ± 9.12	12.35 ± 2.86
12A–12F	111.09 ± 2.7	268.90 ± 28.12	9.41 ± 2.16
12G–12L	114.47 ± 2.59	285.20 ± 6.37	12.49 ± 2.47
14A–14F	94.21 ± 2.17	253.87 ± 5.92	10.49 ± 2.16
14G–14K	92.41 ± 3.16	249.10 ± 8.51	10.60 ± 3.37
13A–13G	109.94 ± 11.92	274.69 ± 29.77	9.56 ± 2.51
13H–13N	111.99 ± 5.69	279.75 ± 14.26	10.44 ± 2.31

certain locations, as shown in the optical macrograph of Fig. 3g. The corresponding scanning electron micrograph, Fig. 6a, reveals the presence of small particles (arrowed) in the fracture surface. A high-magnification fractograph, Fig. 6b, shows how the flow of liquid aluminium (shiny phase) is trapped within some of these oxide particles.

An interesting feature is exhibited in Fig. 6c, where a large particle of spinel (as confirmed by the associated EDX spectrum, Fig. 7) is seen debonded from the surrounding matrix (arrowed). Such a type of decoherence would weaken the alloy, leading to premature failure. Another example of decohesion between oxide particles and the matrix is shown in Fig. 6d, where a lump of wrinkled layers of oxide films is seen. The arrow in Fig. 6d indicates the passage of a crack through the oxide film.

Besides the spinel particles, the other main type of defect observed in the fracture surface is the presence of large volume fractions of Al_2O_3 oxide films, in the form of crumpled layers. These films occur randomly in the melt and, hence, test bars. Fig. 8a and b depict examples of these films near the edge and the centre of the test bar, respectively. The associated X-ray spectrum, Fig. 9, shows strong reflections due to aluminium and oxygen, and a very weak magnesium reflection, indicating the presence of small amounts of MgO and spinel ($MgAl_2O_4$).

The effect of oxide particles or films in weakening the alloy through the initiation of cracks at their interfaces with the matrix is best illustrated by Fig. 10. It is evident from these fractographs that due to the difference in the rigidity (measured by Young's modulus) of the matrix and inclusions, the crack initiates easily at particle/matrix interfaces, leading to rapid crack propagation, large crack paths, and, hence, early failure.

4. Conclusions

4.1. Fresh alloy

1. Under very dry conditions (humidity $\sim$10%–13%), melt cleanliness by sedimentation, i.e. holding

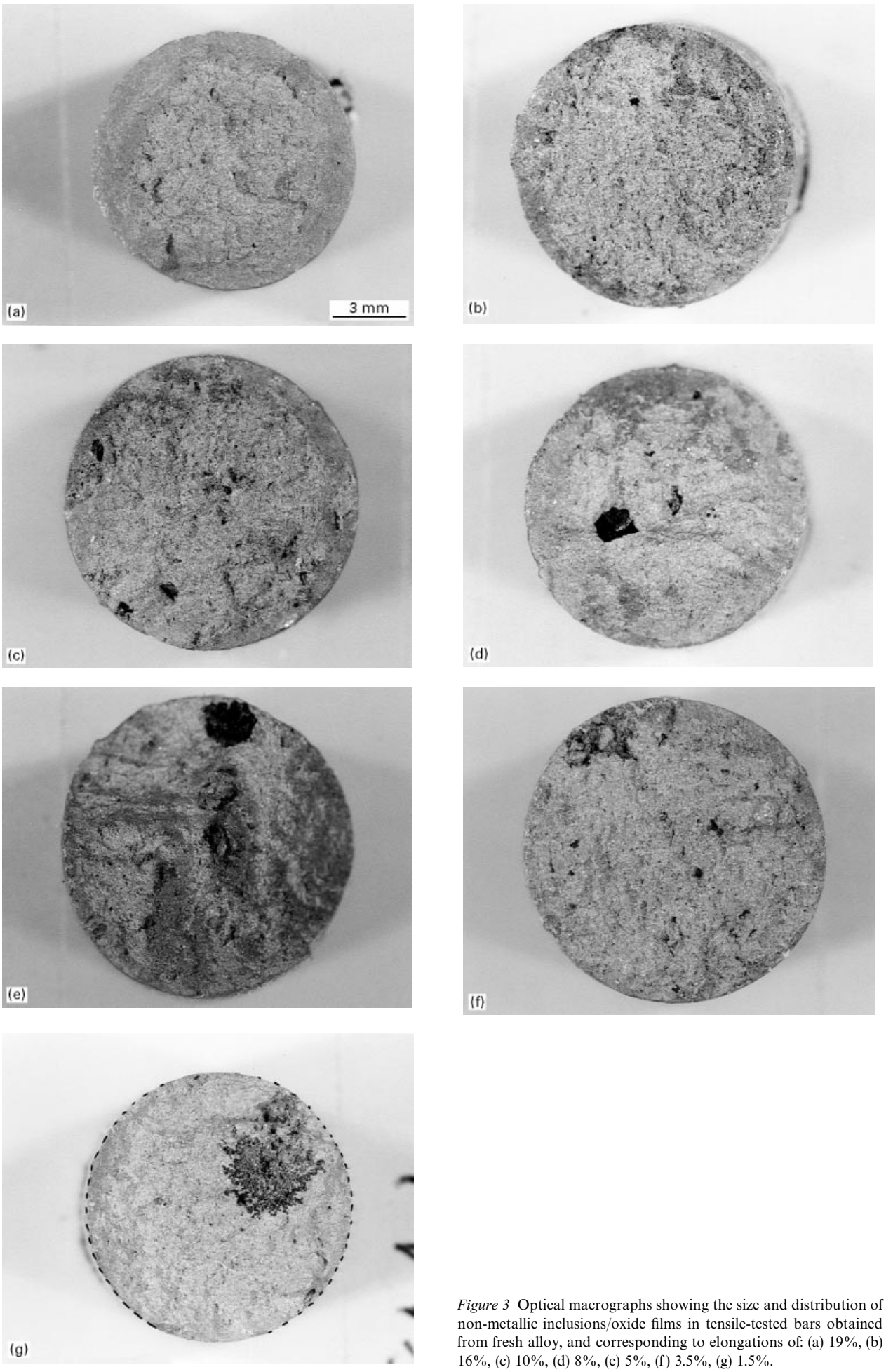

Figure 3 Optical macrographs showing the size and distribution of non-metallic inclusions/oxide films in tensile-tested bars obtained from fresh alloy, and corresponding to elongations of: (a) 19%, (b) 16%, (c) 10%, (d) 8%, (e) 5%, (f) 3.5%, (g) 1.5%.

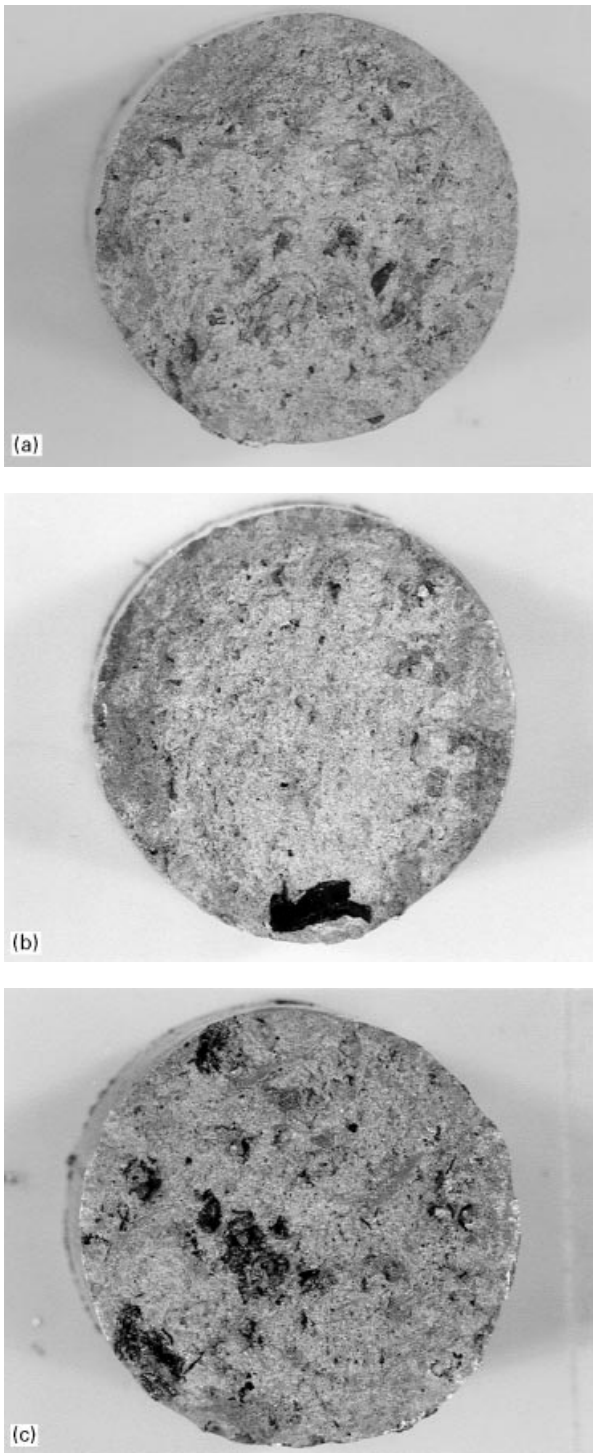

Figure 4 Optical macrographs showing the size and distribution of non-metallic inclusions/oxide films in tensile-tested bars obtained from recycled (scrap) alloy, and corresponding to elongations of: (a) 7.5%, (b) 5%, (c) 3.5%.

the liquid metal at 735 °C for ~72 h, results in the settlement of inclusions to the bottom of the melting crucible, leading to good mechanical properties. Increase in the humidity level, however, will introduce hydrogen to the melt, and result in a large porosity volume fraction deleterious to the mechanical properties.

2. Degassing using a rotary impeller appears to be the most effective method for removing both hydrogen and inclusions, provided it is applied to a reasonably

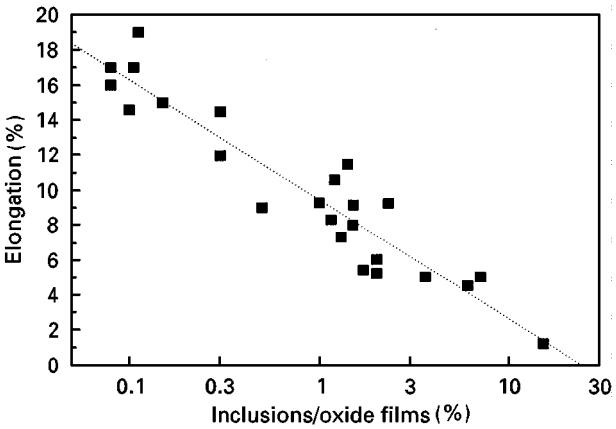

Figure 5 Percentage elongation–log area percentage inclusions/oxide films relationship.

large amount of liquid. The first casting, however, should be rejected, because it is taken from the melt surface layer that is rich in inclusions/oxides.

3. Filtration using 10 or 20 p.p.i. ceramic foam filters is highly recommended for inclusion removal in a dry atmosphere.

4. Mechanical stirring normally used to ensure dissolution of grain refiners or modifiers may be replaced by degassing using a rotary impeller.

5. Oxide films have a much more deleterious effect on the mechanical properties compared to that expected from other inclusions.

4.2. Recycled (scrap) alloy

Holding the liquid metal for a lengthy period of time improves the melt cleanliness similar to that mentioned above. However, due to the presence of excessive amounts of inclusions and oxide films, degassing and/or filtration may be a more appropriate procedure to follow.

In both cases, i.e. fresh and recycled alloys, cracks are initiated at the inclusion (or oxide)–matrix interface, followed by their relatively rapid propagation, leading to the formation of large crack paths through the matrix and, hence, premature failure.

Acknowledgements

This study was supported by several industrial partners (research and development organizations and foundries) in Canada, the United States and Mexico. These include Bomem, Inc. (Québec, Canada), Cercast Group (Québec, Canada), CQRDA (Québec, Canada), FUQAC (Québec, Canada), SÉCAL (Québec, Canada), Grenville Castings Limited (Ontario, Canada), General Motors Powertrain Group (Saginaw, USA), Nemak Corporation (Monterrey, Mexico), KB Alloys, Inc. (Robards, USA), HI-TECH Ceramics (New York, USA). Their financial and in-kind support is gratefully acknowledged. The authors would also like to thank Dr A.M. Samuel for help with the fractography work.

TABLE XVIII Inclusion/oxide–tensile properties relationships for A356.2 alloy

Serial no.	Total inclusion ($mm^2\ kg^{-1}$)	Total harmful inclusion ($mm^2\ kg^{-1}$)	Oxide film classification		YS (MPa)	UTS (MPa)	% Elongation
			Thin	Thick			
1	0.06	0.02	None	None	123.40	310.10	19.20
2	0.02	0.02	Moderate	Moderate	118.54	294.43	14.82
3	0.24	0.02	Moderate	Moderate	116.60	290.61	13.88
4	0.68	0.24	Moderate	Moderate	112.52	281.16	13.38
5	0.17	0.14	Light	Moderate	108.61	271.13	13.16
6	0.54	0.19	Moderate	Moderate	114.45	284.68	13.15
7	0.18	0.15	Light	Light	118.03	294.58	12.66
8	0.03	0.01	Moderate	–[a]	112.25	253.31	12.29
9	0.37	0.22	Light	Light	112.70	280.06	12.26
10	4.24	3.78	None	None	104.35	260.70	11.54
11	0.24	0.19	Heavy	Moderate	111.81	279.28	11.31
12	0.85	0.21	Light	Light	114.00	284.83	10.93
13	0.36	0.29	Moderate	Light	115.47	288.44	10.78
14	0.01	0.00	Heavy	–[a]	112.65	281.34	10.67
15	1.41	1.12	Heavy	Moderate	111.36	278.27	10.60
16	0.64	0.35	Moderate	Moderate	115.59	287.79	10.03
17	1.25	0.36	Moderate	Moderate	114.92	286.61	9.85
18	0.05	0.03	Moderate	Heavy	110.46	276.02	9.32
19	0.03	0.03	Heavy	Heavy	114.80	286.83	9.11
20	0.04	0.01	Moderate	–[a]	106.01	264.83	8.24
21	1.68	0.08	Light	–[a]	113.61	283.79	7.63
22	0.03	0.01	Moderate	–[a]	107.73	244.76	7.21
23	0.10	0.07	Heavy	Heavy	98.39	245.87	7.18
24	0.93	0.48	Moderate	Moderate	109.25	272.51	6.95
25	0.04	0.02	Moderate	Heavy	101.82	254.35	5.36
26	1.40	1.12	Heavy	Heavy	89.40	223.40	1.94

[a] Classification indeterminable.

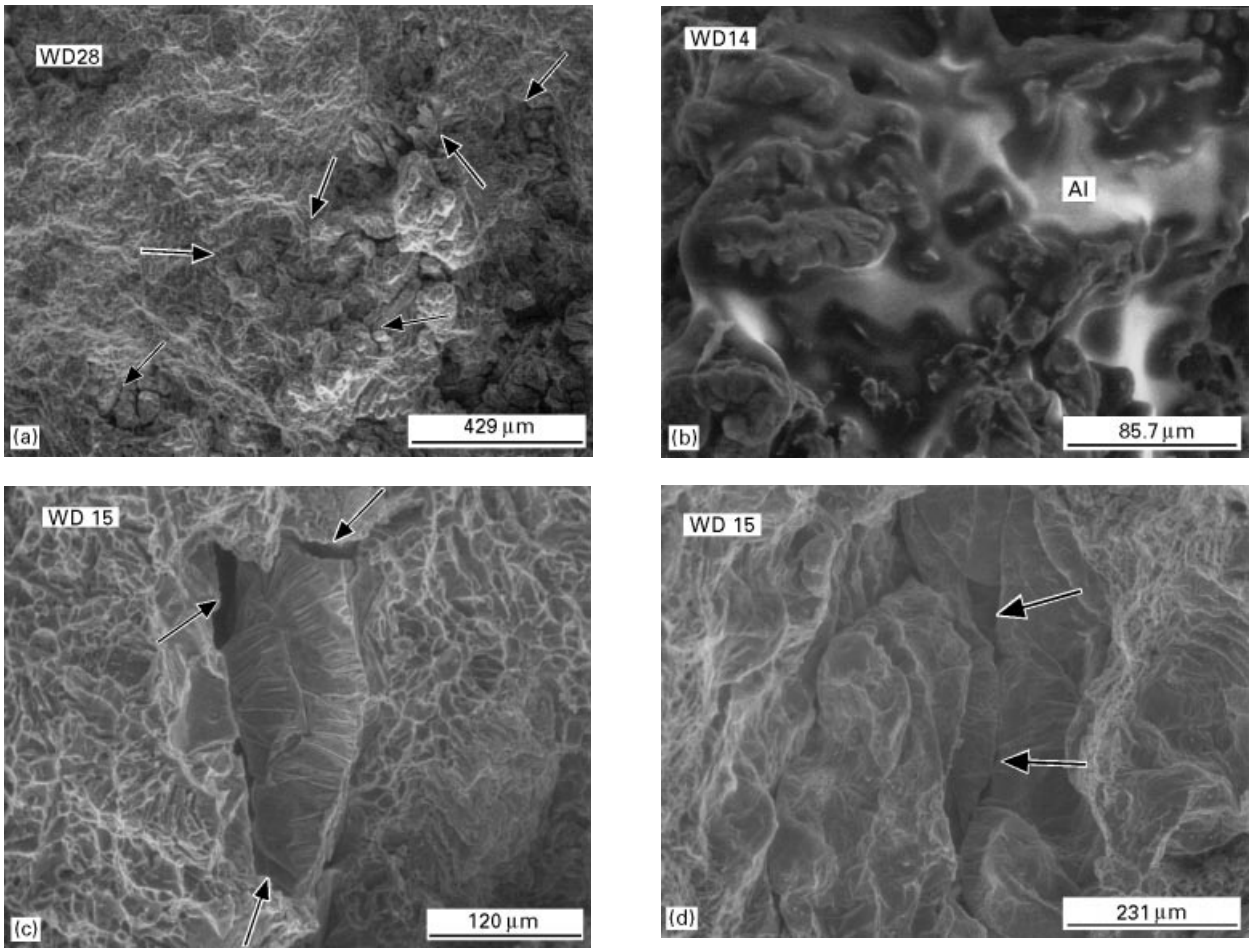

Figure 6 Fracture surface of a tensile-tested bar obtained from an alloy melt held for 72 h at 735 °C, showing: (a) fragmentation of oxide particles (corresponding to Fig. 3g), (b) the presence of liquid aluminium entrapped within oxide film particles, (c) debonding of a large spinel particle from the surrounding matrix, (d) a crumpled mass of oxide films (the arrow denotes the crack path).

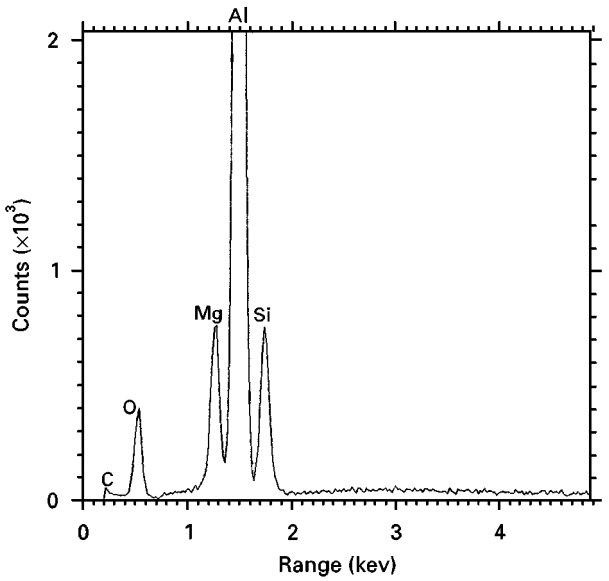

Figure 7 The energy dispersive X-ray (EDX) spectrum corresponding to Fig. 6c, showing strong reflections due to oxygen, magnesium and aluminium.

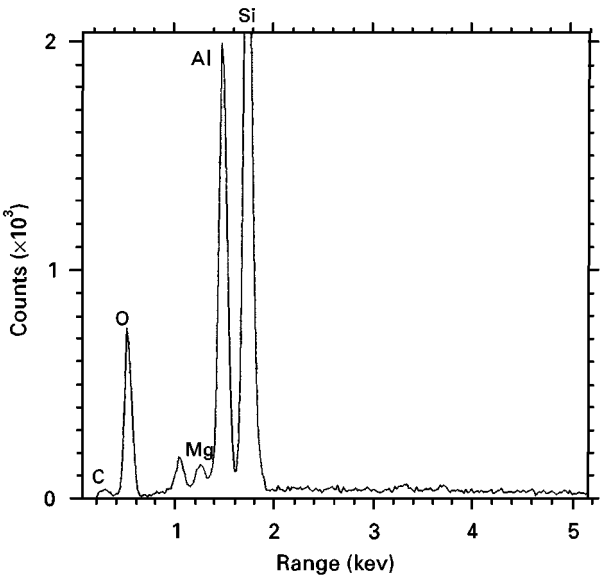

Figure 9 Typical energy dispersive X-ray (EDX) spectrum corresponding to the Al_2O_3 oxide films shown in Fig. 8a. Note the very weak magnesium reflection.

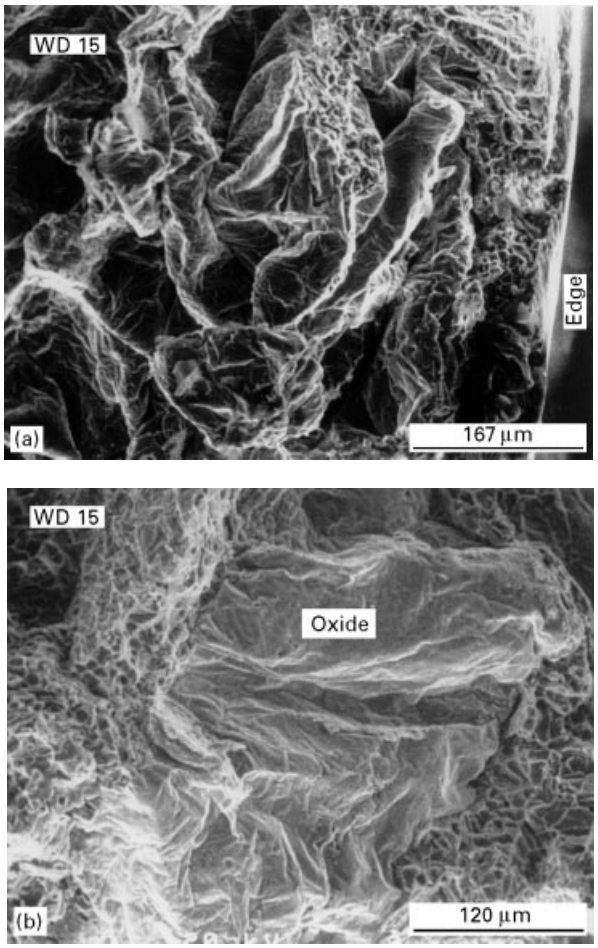

Figure 8 Fracture surface of a tensile tested bar obtained from recycled alloy (Fig. 4c), showing a crumpled mass of oxide films: (a) near the edge, and (b) close to the centre of the test bar.

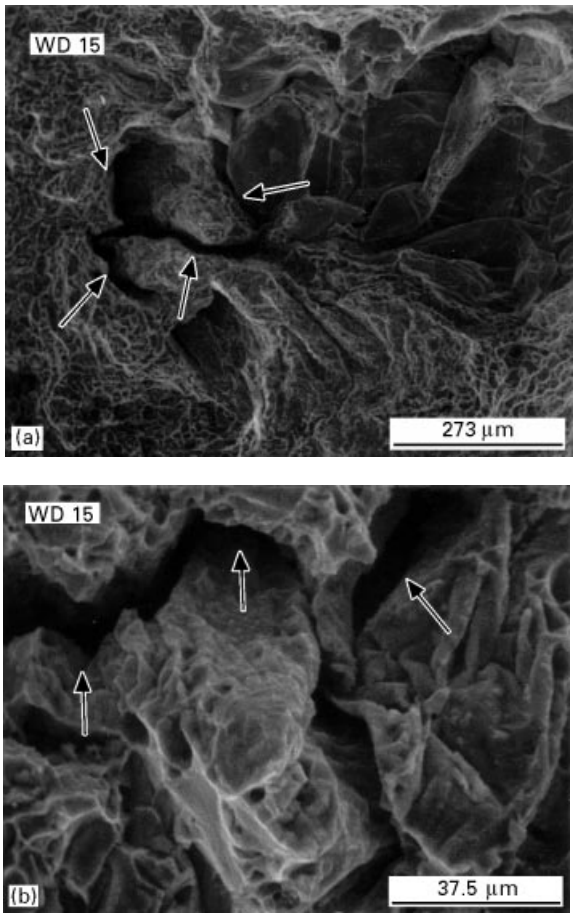

Figure 10 Fracture surfaces showing crack paths located at oxide/matrix interfaces in the samples corresponding to those shown in (a) Fig. 4a, and (b) Fig. 4c.

References

1. W. SIMMONS, *Indian Foundry J.* August (1986) 21.
2. C. J. SIMENSEN and G. BERG, *Aluminium* **56** (1980) 335.
3. D. APELIAN, in "1988 Electric Furnace Conference Proceedings", (Iron and Steel Society, Warrendale, PA, 1989) p. 325.
4. D. APELIAN, R. MUTHARASAN and S. ALI, *J. Mater. Sci.* **20** (1985) 3501.

5. H. C. CUMMINGS, F. B. STULEN and W. C. SCHULTE, *Trans. Amer. Soc. Metals* **49** (1957) 487.
6. C. E. ECKERT, R. E. MILLER, D. APELIAN and R. MUTHARASAN, *Light Metals* (1984) 1281.
7. C. J. SIMENSEN, *Metall. Trans.* **12B** (1981) 733.
8. J. GOBRECHT, *Geisserei* **62** (1975) 263.
9. F. H. SAMUEL, H. LIU and A. M. SAMUEL, *Metall. Trans.* **24A** (1993) 1631.
10. J. E. CAMPBELL, "Castings" (Butterworth-Heinemann, Oxford, 1991).
11. D. HEDJAZI, G. H. J. BENNETT and V. KONDIC, *Metall. Technol.* **3** (1976) 537.
12. *Idem*, *Br. Foundryman* **68** (1975) 305.
13. K. ARAI, T. ONISHI, M. GOTO and R. OTSUKA, *J. Jpn Inst. Light Metals* **27** (1977) 319.
14. P. R. RIOS, J. C. BRUNO and A. S. M. FONSECA, *J. Mater. Sci. Lett.* **10** (1991) 1346.
15. K. H. CHIEN, T. Z. KATTAMIS and F. R. MOLLARD, *Metall. Trans.* **4A** (1973) 1069.
16. V. GEROLD, in "Fourth International Conference on Age-Hardenable Aluminium Alloys", Balatonfured, Hungary, May 1985, Materials Science Forum 13–14 (1987) pp. 175–94.
17. C. E. ECKERT, R. E. MILLER, D. APELIAN and R. MUTHARASAN, *Light Metals* (1984) 1281.
18. D. APELIAN and R. MUTHARASAN, *J. Metals* **32** (1980) 14.
19. D. APELIAN and R. MUTHARASAN, "Modelling of Inclusion Removal of Melt Systems", presented at the 72th Annual AIChE Meeting, San Francisco, CA, November 1979.
20. C. J. SIMENSEN and U. HARTVEDT, *Z. Metallkde* **76** (1985) 409.
21. L. J. GAUCKLER, M. M. WEBER, C. CONTI and M. JACOB-DULIERE, *Light Metals* (1985) 1261.
22. T. CALLAIS, M. RICHARD and M. STUCKY, *Fonderie-Fondeur d'aujourd'hui* **97** (1990) 22.
23. L. F. MONDOLFO, "Grain Refinement in Castings and Welds" (Metallurgical Society of AIME, 1983) pp. 3–50.
24. M. M. GOZOWSKI, D. A. SENTER and G. K. SIGWORTH, *Metall. Trans.* **18A** (1987) 603.
25. G. K. SIGWORTH and M. M. GOZOWSKI, *Amer. Foundrymen's Soc. Trans.* **93** (1985) 907.
26. S. KENNERKNECHT, in "Advanced Casting Technology", AGARD Conference Proceedings No. 325, Advisory Group for Aerospace Research and Development, North Atlantic Treaty Organization [AGARD/NATO], Brussels, Belgium, 4–9 April 1982, pp. 1–52.
27. S. Z. LU and A. HELLAWELL, *Metall. Trans.* **18A** (1987) 1721.
28. D. APELIAN, G. K. SIGWORTH and K. R. WHALER, *Amer. Foundrymen's Soc. Trans.* **92** (1988) 297.
29. R. DASGUPTA, C. G. BROWN and S. MAREK, *ibid.* **96** (1988) 297.
30. P. D. HESS and E. V. BLACKMUN, *ibid.* **84** (1975) 87.
31. M. GARAT and R. SCALLIET, *ibid.* **84** (1978) 549.
32. L. LIU and F. H. SAMUEL, *J. Mater. Sci.* **33** (1997) 5901.
33. *Idem*, *ibid.* **33** (1997) 5927.

Received 5 August
and accepted 17 December 1997